AGU100 ADVANCING EARTH AND SPACE SCIENCE

Water Resources Research

RESEARCH ARTICLE
10.1029/2017WR022177

Formation, Growth, and Failure of Debris Jams at Bridge Piers

Diego Panici[1] **and Gustavo A. M. de Almeida**[1]

[1] Faculty of Engineering and the Environment, University of Southampton, Southampton, UK

Key Points:
- Experimental results show that the growth of debris jams at piers is halted at a critical stage
- New relations are proposed between the size of debris jams and flow and debris variables
- Accumulations formed with uniform are considerably larger than with nonuniform debris

Correspondence to:
D. Panici,
d.panici@soton.ac.uk

Citation:
Panici, D., & de Almeida, G. A. M. (2018). Formation, growth, and failure of debris jams at bridge piers. *Water Resources Research*, *54*. https://doi.org/10.1029/2017WR022177

Received 7 NOV 2017
Accepted 9 AUG 2018
Accepted article online 24 AUG 2018

Abstract The accumulation of large wood debris around bridge piers obstructs the flow, producing increased upstream water levels, large horizontal structural loadings, and flow field modifications that can considerably exacerbate scour. These effects have frequently been held responsible for the failure of a large number of bridges around the world, as well as for increased risk of flooding of adjacent areas. Yet little is currently known about the time evolution and processes responsible for the formation and growth of these debris piles. This paper is aimed at deciphering the whole life of debris accumulations through an exhaustive set of 570 experiments in which debris elements were individually introduced into a flume and accumulated at a pier model downstream. Our findings show that in all experiments, the growth of accumulations is halted at a critical stage, after which the jam is removed from the pier by the flow. This condition typically coincides with the time when the dimensions of the accumulations are maxima. The values of the accumulation maximum size display a clear dependence on flow characteristics and debris length distribution. On the other hand, other variables have shown much weaker effects on the geometry of the accumulations. For a given debris length, accumulations are wide, shallow, and long at low flow velocities but become narrower, deeper, and shorter with increasing velocities. A comparison of results of accumulations formed with debris of uniform and nonuniform size distributions has revealed that the former can be up to 2.5 times wider than the latter.

1. Introduction

Engineers, scientists, and the lay public alike have long been troubled by the complex and sometimes catastrophic interplay between rivers and bridges. Bridge piers alter the flow field, inducing hydraulic loadings on the structure and scour of the river bed, which combined have historically led to the failure of many bridges worldwide. In addition, the resulting rise in upstream water levels can significantly increase the risk of flooding of adjacent areas. These effects are often complicated and magnified by other phenomena that inherently take place in rivers and produce further alterations to flow and sediment dynamics. Among these, the accumulation of large wood debris (hereafter referred to as LWD, wood in rivers, instream wood, or simply debris) at piers is being increasingly acknowledged as a key mechanism affecting the way that bridges interact with rivers and respond to floods (Benn, 2013; Bradley et al., 2005; Diehl, 1997; Lagasse et al., 2010).

Many rivers mobilize and transport large volumes of LWD during flood events (Lyn et al., 2003; Ruiz-Villanueva et al., 2016; Sedell et al., 1988). Obstacles within the path of instream wood such as a bridge pier can entrap incoming logs and initiate the formation and subsequent growth of a LWD pile (Diehl, 1997). Field observations suggest that these accumulations usually begin with a key element, that is, a large and sturdy log (Bradley et al., 2005; Diehl, 1997; Lagasse et al., 2010). This key element then collects other logs or smaller drift material, accelerating the growth of the debris pile (Abbe & Montgomery, 1996; Lagasse et al., 2010; Manners et al., 2007). In situ observations also indicate that an inverted half cone (Diehl, 1997; Lagasse et al., 2010) or a pointing arrow (Abbe & Montgomery, 1996) is the most common accumulation shape, although other shapes have also been observed (Lagasse et al., 2010).

Once formed, debris jams can significantly contribute to structural failure and increased flood risk in different ways. First, the drag force that is exerted on the debris and transferred to the pier can be an order of magnitude larger than the corresponding drag exerted by the flow on the pier alone. Second, the reaction force applied by the debris on the flow, combined with the reduction in the flow area, is usually responsible for substantial increases in upstream flood levels (Gippel et al., 1996; Parola et al., 2000) often referred to as afflux. Third, the presence of debris further modifies the flow field and exacerbates scour (Lagasse et al., 2010; Melville & Dongol, 1992; Pagliara & Carnacina, 2011, 2013). Diehl (1997) indicates that debris accumulations at piers

contribute to more than one third of bridge failures in the United States, and other examples of the relevance of debris-induced bridge failures around the world are also abundant (e.g., Benn, 2013).

In spite of the crucial role played by instream debris in increasing the risk of bridge failure and flooding, scientific studies on the dynamics of debris accumulations at bridge piers are still scarce. Most research hitherto conducted on debris interactions with bridges has focused on quantifying the potential increase in scour induced by debris jams. These studies have assumed different shapes, dimensions, porosities, and roughness of laboratory models of debris jams, which have been tested under a range of flow conditions to determine their potential effects in increasing scour (Lagasse et al., 2010; Melville & Dongol, 1992; Pagliara & Carnacina, 2011). This approach disregards the potential relation between the flow conditions and the size of the formed debris accumulations and is likely to produce unrealistic estimations of the maximum scour that can possibly develop. Although debris accumulations have been experimentally formed previously (Bocchiola et al., 2008; Lyn et al., 2003; Rusyda et al., 2014), this type of studies has so far been limited in scope and has not attempted to decipher the intrinsic relations between flow and the corresponding characteristics of the formed debris jams. Lyn et al. (2003) performed repeated experiments in a 0.4-m-wide flume whereby natural twigs were individually introduced upstream of a pier model and analyzed the probability that a stable jam could be formed. Bocchiola et al. (2008) studied the entrapment of debris (modeled using cylindrical dowels) by an array of 156 randomly distributed vertical rods. Rusyda et al. (2014) modeled accumulations at two Japanese bridges (with and without pier) by instantaneously releasing a large bundle (the number of elements per bundle ranged from 50 to 800) of debris (modeled by dowels) into a 0.3-m-wide flume. Other experiments were focused on the probability of entrapment of individual debris elements (Schmocker & Hager, 2011) or probability of clogging at bridge decks (Gschnitzer et al., 2017) or piano key weirs (Pfister et al., 2013), relating this to debris size, flow conditions, and the presence of rootstocks or branches.

To date, the underlying mechanisms governing the formation and growth of debris jams at single piers, as well as the dependency of key variables such as shape and dimensions on flow and debris characteristics, remain largely unknown. This knowledge gap sets limits to our ability to accurately assess the effects of debris on bridge stability and flooding. While a few methodologies have been proposed to estimate the potential size and shape of large wood accumulations at bridges, their recommendations differ widely, and it is often unclear how they have been obtained or defined (Diehl, 1997). For instance, Australian design practice has recommended 20-m-wide and 1.2-m-deep rectangular-shaped accumulations, while in New Zealand, a triangular shape of 15-m wide and 3-m deep has been suggested (Diehl, 1997). In the United States, guidelines for the assessment of debris accumulations at bridges suggest a design width equal to the length of a key design log, defined as length of the largest sturdy logs (although other factors that may limit the ability of the river to transport large elements are also considered, such as the width of the channel). In addition, a conservative approach is proposed, whereby the width of the accumulation is assumed constant over the full flow depth (Bradley et al., 2005; Diehl, 1997; Lagasse et al., 2010).

Developing a detailed understanding of the processes and relations governing the shape and dimensions of debris jams could pave the way for improved assessment of the consequences of debris on bridge stability and flooding. For example, hydraulic loading could be directly obtained for predicted shapes and dimensions of debris jams using estimated or previously published values of the drag coefficient. The increase in water levels induced by debris blockage could also be readily computed from elementary momentum conservation principles. In addition, knowledge of flow-dimensions relations can pave the way to the design of improved laboratory experiments of debris-induced scour, leading to more accurate scour prediction models.

The aim of this article is to experimentally study the formation and growth of woody debris jams at piers to unveil dependencies between the dimensions and shape of LWD jams and variables describing the characteristics of flow and debris. The article also aims to provide practical relations for the estimation of maximum size of debris jams, as well as the corresponding force that is exerted by accumulated debris on piers. Our focus is limited to single-pier accumulations, defined as the condition when the gap between the pier and nearby elements (such as an abutment, another pier, or the banks of the channel) is large compared to the half width of the debris jam. Single-pier debris accumulation has been recognized as the most common problem found in all regions of continental United States (Lagasse et al., 2010). In addition, single-pier accumulations that do not interact with neighboring boundaries are conceptually simpler than span blockages and therefore represent an excellent starting point to understand the dynamics of their formation and growth without additional complicating phenomena. In our experiments the single-pier condition has been enforced by using a

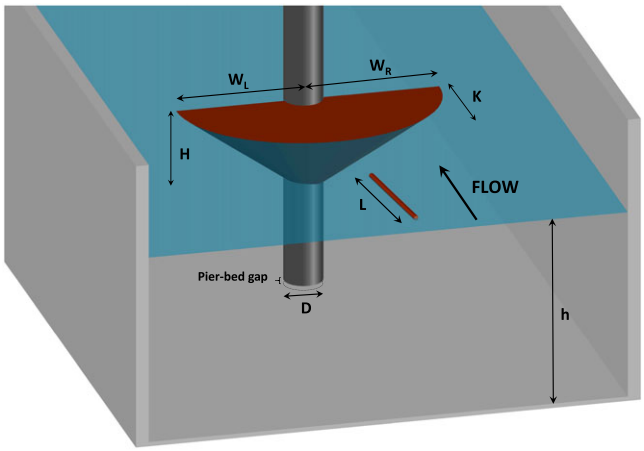

Figure 1. Idealized three-dimensional sketch of a debris jam, with indication of the main geometrical characteristics involved.

relatively wide flume (1.375 m) with a centrally positioned single pier and through careful manipulation of experimental variables. A total of 570 experiments were performed. The dynamics of debris accumulations and the size reached by LWD piles for a range of flow conditions was analyzed by individually introducing natural sticks into the channel upstream from the pier. The time evolution of the accumulation was examined initially, which unveiled clearly distinct stages that were then used to define maximum potential dimensions. Second, we analyzed the influence of length, diameter, and density of debris elements, water depth, and pier size on the dimensions of accumulations for the idealized situation of uniform size debris. Finally, comparisons were drawn between accumulations formed with uniform and nonuniform length debris, the latter providing a more realistic representation of debris supply that is typically observed in natural environments. This study follows a preliminary work by Panici and de Almeida (2017) which was based on a reduced data set.

2. Dimensional Analysis

Dimensional analysis was performed in order to define a functional relation between the dimensionless variables that are effectively significant to the phenomenon of woody debris accumulations. Furthermore, dimensional analysis ensures similarity between laboratory and prototype (i.e., real-world) scales when dimensionless parameters are equal in both model and prototype. Thus, the following functional relationship between fluid, flow, and debris variables is proposed:

$$f\left(\rho, \mu, v, h, g, D, L, d, \rho_L, B, W, H, K\right) = 0, \tag{1}$$

where ρ is the water density, μ is the dynamic viscosity of water, v is the streamwise component of cross-section-averaged velocity approaching the LWD jam (prior to the formation of the accumulation), h is the water depth, g is the acceleration due to gravity, D is the diameter of the pier, L and d are, respectively, the length and diameter of individual debris elements (i.e., a natural stick), ρ_L is the debris density, B is the width of the flume, and W, H, and K are, respectively, width, height, and length of the debris accumulation (as illustrated in Figure 1). As two variables W and K are used to describe the planar geometry, the jam shape is not restricted to a semicircular cone. Equation (1) can then be rearranged in a more compact and dimensionless form by applying Buckingham π theorem. For the woody debris problem, we chose ρ, v, and L as the repeating variables yielding the following functional relationship between ten dimensionless variables:

$$g\left(Re_L, Fr_L, \frac{h}{L}, \lambda, \frac{d}{L}, \frac{\rho_L}{\rho}, \frac{B}{L}, \omega, \eta, \kappa\right) = 0, \tag{2}$$

where $Re_L = \frac{\rho v L}{\mu}$ and $Fr_L = \frac{v}{\sqrt{gL}}$ are, respectively, the debris Reynolds and debris Froude numbers (i.e., using L as the characteristic length), $\lambda = \frac{L}{D}$ is the dimensionless length of individual debris elements with respect to the pier size, and $\omega = \frac{W}{L}$, $\eta = \frac{H}{L}$, and $\kappa = \frac{K}{L}$ are the three dimensionless variables used to describe the geometry of the accumulation. The Reynolds number was assumed to have only a negligible effect on the process of debris accumulation (i.e., Reynolds invariance is assumed), so that Re_L was dropped from (2) resulting in:

$$g\left(Fr_L, \lambda, \frac{d}{L}, \frac{h}{L}, \frac{\rho_L}{\rho}, \frac{B}{L}, \omega, \eta, \kappa\right) = 0. \tag{3}$$

The functional relationship (3) relates the three variables characterizing the geometry of a debris jam ($\omega, \eta,$ and κ) to variables that describe the characteristics of both flow and individual debris elements. Experiments and data analysis were performed according to these dimensionless variables as found in (3).

3. Experiments

The experimental work was conducted in a 22-m-long and 1.375-m-wide glass-walled rectangular tilting flume. Figure 2 illustrates (not to scale) the flume used and the experimental setup adopted. Water was pumped from a sump located underneath the flume by three pumps with capacity of delivering

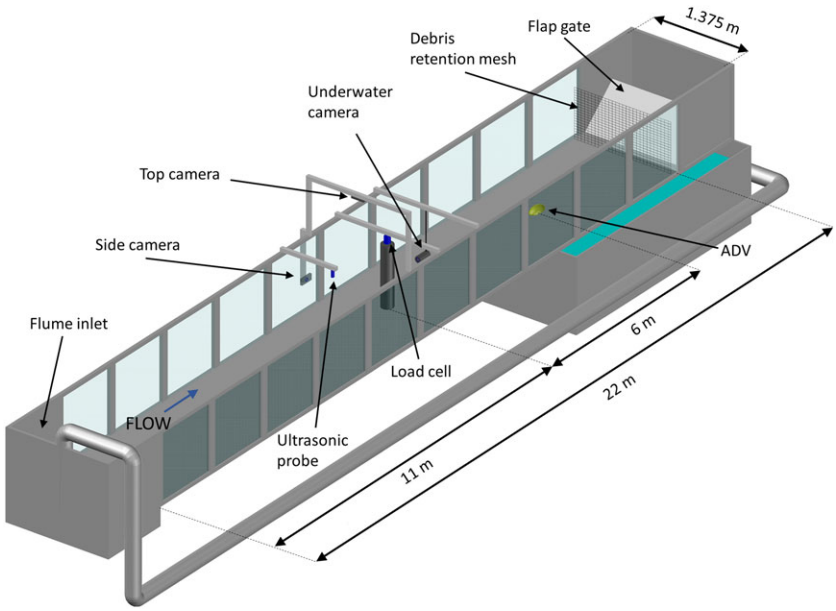

Figure 2. Sketch of the flume setup showing the position of the instruments used (not to scale). Sumps and pipes connections are simplified for ease of representation.

discharges from 0.08 up to 0.42 m^3/s. Each debris-pier configuration was tested under at least 15 different flow discharges and water depths, resulting in velocities within the range 0.22 to 0.92 m/s. All tests were carried out under steady and subcritical flow conditions. Reynolds number $Re = \rho vh/\mu$ ranged from 5.10×10^4 to 3.06×10^5. Water depths at the pier section were controlled by a flap gate installed at the downstream end of the flume. Bridge piers were modeled using three 600-mm-long solid polyvinyl chloride cylinders with diameters of $D = 25$, 50, and 100 mm. The piers were installed 11-m downstream from the inlet at the centerline of the flume. Previous studies conducted in this flume have determined that the flow is fully developed at this location. Discharge was measured continuously during each experiment by a multicell multibeam ADV SonTek IQ Plus® installed 6-m downstream of the pier, which also recorded water depth and temperature. Water level was continuously monitored by an ultrasonic sensor (accuracy ±0.2% of the range, frequency 10 Hz) placed 1-m upstream of the pier.

A load cell Thames Side T66® was attached to the top end of the pier to measure the force exerted by flow and debris on the pier in the streamwise direction. The load cell used had a 50 kg capacity, maximum error of 0.017% of the capacity, and sampling rate of 10 Hz. To avoid loss of measured load due to friction between pier and flume bed, a small gap of approximately 0.5 mm was left between the pier and bottom of the flume. In order to provide an accurate estimation of the drag coefficient, previous studies have partitioned the force exerted on the pier into drag and static components. The latter results from the difference in the hydrostatic forces induced by the drop in the free surface from upstream to downstream. Parola et al. (2000) estimated this static component as the hydrostatic force that would be exerted on a solid block with the same dimensions as the debris accumulation. Applying this partitioning method to our experimental results (i.e., using measurements of water levels upstream and downstream from the debris jam) resulted in a static component that was on average 0.54% of the total force. For simplicity, this static force component was assumed negligible, and the measured force was assumed to represent the drag force only. In order to understand the effects of debris on loadings, the total drag force measured F_{Dt} must be decomposed into the drag force exerted on the debris F_{Dd} plus the drag exerted on the part of the pier that is below the accumulation F_{Dp}:

$$F_{Dt} = F_{Dd} + F_{Dp}. \tag{4}$$

The term F_{Dp} was estimated for each experiment using Reynolds dependent values of the drag coefficient for cylindrical bodies from the literature (Tritton, 1977) and the approach flow average velocity v_{ap}. This simplified approach (also adopted by Parola et al., 2000; Hygelund & Manga, 2003; Manners et al., 2007) is, however, only an approximation, as the flow field under the debris jam is complex (Pagliara & Carnacina, 2013). Nevertheless, measurements of velocity close to the pier by intrusive methods available were not possible as they would

Table 1
Debris Characteristics for Uniform Length (U1 to U5), Nonuniform Length (N1 to N13), Varied Diameter (D1 to D6), Varied Water Depth (H1 to H3), Varied Debris Density (T1 and T2), and Repeated (R1) Experiments

Group	L (mm)	d (mm)	D (mm)	h range (mm)	Number of experiments	Fr range	Fr_L range
U1	375.0	11.85	100	282–461	18	0.16–0.43	0.14–0.43
U2	250.0	11.85	50	296–395	21	0.13–0.42	0.14–0.51
U3	312.5	11.85	50	296–396	21	0.13–0.42	0.12–0.47
U4	375.0	11.85	50	260–394	19	0.15–0.43	0.12–0.43
U5	375.0	11.85	25	282–420	18	0.16–0.44	0.14–0.43
D1	375.0	7.64	50	285–377	21	0.14–0.51	0.13–0.48
D2	375.0	9.65	50	285–377	21	0.14–0.52	0.13–0.48
D3	375.0	14.85	50	285–377	21	0.14–0.51	0.13–0.47
D4	375.0	17.85	50	286–377	21	0.14–0.51	0.13–0.48
D5	375.0	21.59	50	286–377	21	0.14–0.51	0.13–0.48
D6	375.0	29.26	50	295–394	21	0.13–0.42	0.12–0.42
H1	375.0	11.85	50	290–299	20	0.13–0.46	0.12–0.41
H2	375.0	11.85	50	366–373	21	0.12–0.43	0.11–0.43
H3	375.0	11.85	50	442–454	17	0.10–0.32	0.11–0.35
T1	375.0	11.85	50	288–377	21	0.14–0.51	0.12–0.41
T2	375.0	11.85	50	288–377	21	0.14–0.52	0.11–0.43
N1	500.0	11.37	100	268–402	17	0.16–0.42	0.11–0.35
N2	625.0	11.38	100	268–407	18	0.16–0.43	0.10–0.33
N3	375.0	10.86	50	268–412	15	0.15–0.42	0.13–0.40
N4	437.5	10.65	50	268–409	16	0.15–0.42	0.12–0.38
N5	500.0	11.37	50	275–408	18	0.15–0.43	0.11–0.37
N6	562.5	11.40	50	277–405	18	0.15–0.44	0.11–0.35
N7	625.0	11.38	50	274–408	18	0.15–0.43	0.10–0.33
N8	687.5	11.65	50	271–405	17	0.15–0.43	0.09–0.32
N9	750.0	11.35	50	271–405	18	0.15–0.44	0.09–0.30
N10	437.5	10.65	25	274–400	16	0.16–0.43	0.13–0.37
N11	500.0	11.37	25	274–401	18	0.16–0.44	0.12–0.38
N12	625.0	11.38	25	274–409	18	0.16–0.44	0.10–0.34
N13	750.0	11.35	25	274–402	18	0.15–0.42	0.09–0.30
R1	687.5	11.65	50	355–365	22	0.23–0.24	0.17–0.18

have disturbed the flow and influenced the process of growth of the jam. The estimated values of F_{Dd} thus obtained were used to determine the drag coefficient of the debris:

$$C_{Dd} = \frac{4F_{Dd}}{\rho W H v_{ap}^2}. \tag{5}$$

All tests were continuously recorded by three cameras. The first camera was placed above the flume and 0.70-m upstream from the pier, whereas a second camera of the same characteristics was placed on the external side of the flume 0.30-m upstream from the pier. A cylindrical submerged camera held by a thin bar was placed 0.60-m downstream of the pier. Its size (a diameter of 35 mm) and shape were chosen to minimize the alterations on the upstream flow conditions. Together, these three cameras provided a detailed description of the time evolution of the shape and size of the accumulation in three dimensions (represented by the geometrical variables width W, height H, and length K). Size measurements were made possible by using a reference mesh, the image of which was captured prior to each experiment. For the top camera, we used a ruled paper with a square mesh of 10-mm side, which was positioned at different elevations in order to account for depth variations during the experiments. To account for refraction effects, a wired square mesh of 12.7-mm side was submerged to serve as a reference for the other two cameras.

The experiments were conducted by introducing individual debris elements into the flume at a distance of 7-m upstream of the pier. Debris elements were manually dropped onto the water surface at a distance of approximately 50 mm and released parallel to the streamwise direction, reproducing the mode of transport of individual logs observed in natural streams (Diehl, 1997). The dropping point was at the flume centerline, after which debris elements were left free to move with the current, remaining at the water surface. A dropping frequency of approximately 20 debris per minute was used in all experiments, which represents the *uncongested* mode of debris transport (defined by Braudrick et al., 1997, as the condition when logs or branches are transported individually rather than in clusters). This type of transport has been previously described as the most commonly observed in rivers (Braudrick et al., 1997; Lyn et al., 2003). The analysis of video recordings of a preliminary set of tests indicated that in *uncongested* mode of transport, the debris dropping frequency could change the speed of the growth but would not significantly change the final dimensions of the formed debris piles. We have therefore kept the dropping frequency constant for all experiments and focused on the analysis of other variables that were deemed to play a more important role on the final dimensions. In experiments with high flow velocity, a small number of debris elements needed to be manually placed at the pier in order to initiate an accumulation, which would otherwise have taken too long to form by the stochastic process of self-assembly observed in the other experiments. This operation was conducted only for a reduced number of experiments and only to initiate the accumulation process. Debris elements that did not accumulate around the pier and continued to move along the flume were collected by a wire mesh screen located close to the flume outlet. These were frequently removed from the mesh over the course of each experiment to avoid backwater effects that might affect the depth at the pier section. Experiments were stopped when the accumulation failed (i.e., was dislodged from the pier, as will be discussed later).

In order to represent shape irregularities commonly observed in debris found in natural environments, natural sticks (twigs and branches fallen from trees) were used to model LWD, as also previously recommended by Lyn et al. (2003). The average density of this material was kept approximately constant throughout all tests by drying the sticks after each experiment. All sticks used were defoliated, with neither branches nor root wads. Two different sets of model debris were used: uniform and nonuniform (i.e., distributed) length sticks. Debris length and pier diameter (as well as other variables describing debris and flow) for each group of experiments are indicated in Table 1. All experiments (except for groups T1 and T2) were carried out with densities between 450 and 550 kg/m^3.

For uniform debris, 16 groups of experiments were conducted. The first five groups (U1 to U5 in Table 1) were performed with different values of the relative debris length λ in order to study the influence of this variable on the characteristics of the formed debris jams. In these experiments the diameter d of individual debris members (measured using a digital calliper) was kept relatively constant (i.e., maximum coefficient of variation 10.5%), whereas the pier diameter D was varied. The values of λ tested ranged from 3.75 to 15 which are representative of typical values observed in natural environments (Lagasse et al., 2010). Groups of experiments D1 to D6 tested the effects the dimensionless variable d/L on the debris accumulation by keeping the debris length L constant and varying the debris diameter d for each group. The range of values of d/L (also considering groups U1 to U5 where L was varied and d kept constant) was $0.020 \leq d/L \leq 0.078$. Experimental groups H1 to H3 were aimed at analyzing the influence of the dimensionless variable h/L. In these experiments L and h were kept constant within each group, but h had a different value for each group. This resulted in three different h/L values of 0.783, 0.985, and 1.195. Prior to each of these tests of the H1 – H3 groups, the slope of the flume was gradually adjusted until the uniform flow depth of the group was achieved. The nonzero slope also allowed uniform flow conditions to be established, which was achieved by adjusting the position of the downstream gate. All other groups of tests were performed with the flume horizontal. For these tests with horizontal flume, the long distance from the flume outlet to the pier ensured that the values of the convective accelerations were negligible (values ranged between 5.89×10^{-6} and 5.01×10^{-4} m/s^2) compared to the flow accelerations induced by the debris and pier. Experiments in groups T1 and T2 were performed with two different debris densities, respectively, 396 and 860 kg/m^3. Density was kept under control by either drying or soaking sticks. For debris elements of T1 group, sticks were dried by a drying system until reaching a minimum, constant density. On the other hand, debris of the T2 group were left into a water tank overnight and then tested on the following day.

Field observations of woody debris accumulations suggest that LWD jams are typically formed by elements, the length of which is nonuniformly distributed (Blersch & Kangas, 2014; Sedell et al., 1988), that is, the length of individual debris can significantly vary within the same jam. It has been usually reported that accumulations

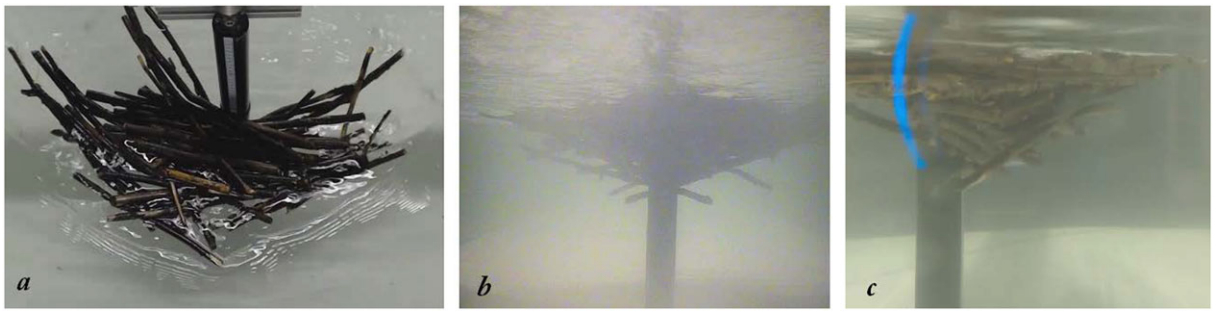

Figure 3. Typical accumulation shape during the stable phase for a nonuniform size debris test (L = 500 mm, D = 50 mm, v = 0.411 m/s resulting in λ = 10, and Fr_L = 0.186). Images were captured at the same instant from (a) top camera, (b) underwater camera located downstream from the pier, and (c) side camera.

are initiated by a key element (the longest woody debris) and then completed by smaller pieces (Diehl, 1997; Lagasse et al., 2010; Manners & Doyle, 2008; Manners et al., 2007). In order to mimic these observations, a set of 13 distributed debris mixtures was produced, each of which was characterized by the length of the longest element (Table 1, groups N1 to N13). Within each group, smaller elements were added to complete the distribution according to typical woody debris distributions observed in rivers. Debris lengths in rivers are usually nonnormally distributed (Blersch & Kangas, 2014) and skewed toward smaller sizes. In order to produce a length distribution that mimics these observed characteristics, published data (Hess, 2007) of debris lengths found in the South River (Virginia, United States) were used to fit a log-normal probability density function:

$$p(\varepsilon) = \frac{1}{\varepsilon\sqrt{2\pi}\sigma} e^{-\left(\frac{\ln\varepsilon-\mu}{\sqrt{2}\sigma}\right)^2}, \tag{6}$$

where ε is the ratio between the length of individual debris elements L_i and the length of the key element L_{key}, and μ and σ are, respectively, the mean and standard deviation of $\ln\varepsilon$. The values of the parameters were determined by regression analysis as $\mu = -1.3039$ and $\sigma = 0.7367$. The resulting distribution also displayed a similar trend to that described in Sedell et al. (1988), which was based on about 2,000 observations of debris lengths. The probability density function (6) was then discretized into 10 class intervals within the range $0 < L_i/L_{key} \leq 1$, and the frequency p_i of each size class was determined as

$$p_i = \frac{1}{\Delta\varepsilon}\int_{\varepsilon_{1_i}}^{\varepsilon_{2_i}} p(\varepsilon)d\varepsilon, \tag{7}$$

where $\Delta\varepsilon = 0.1$, and ε_{1_i} and ε_{2_i} are, respectively, the width and the two limits of each class interval. Equation (7) was used to determine the number of debris elements within each size class, the corresponding length of which is defined by the average of the class interval $L_i = L_{\text{key}}\frac{\varepsilon_{1_i}+\varepsilon_{2_i}}{2}$. In the analysis of the results of these experiments with nonuniform length debris, the value of L used in the dimensionless parameters of equation (2) is the length of the key element L_{key}. During these tests, the key element was placed at the pier prior to each experiment, in order to ensure that this element started the accumulation and acted as the main recruiter of other smaller pieces.

Finally, an experiment arbitrarily chosen from the nonuniform group N8 was repeated 22 times with the same flow and debris characteristics in order to analyze the randomness of the process of growth of debris accumulations (R1 in Table 1).

4. Results

As previously observed by Panici and de Almeida (2017), the evolution of debris accumulations observed in all experiments presented here repeatedly showed a similar pattern that can be conceptually classified as three different phases, hereafter referred to as *unstable*, *stable*, and *critical*. At the beginning of the build-up process, the debris pile is formed by only a few elements that are anchored to the pier at the water surface. These members significantly increase the width of the debris recruiting area, resulting in a rapid increase of the three geometrical variables W, H, and K as well as of the force exerted onto the pier. During this initial development, which we classified as unstable, debris can be easily detached from the jam either individually or in clusters resulting in frequent variations of the geometrical variables or even in an early jam failure. After

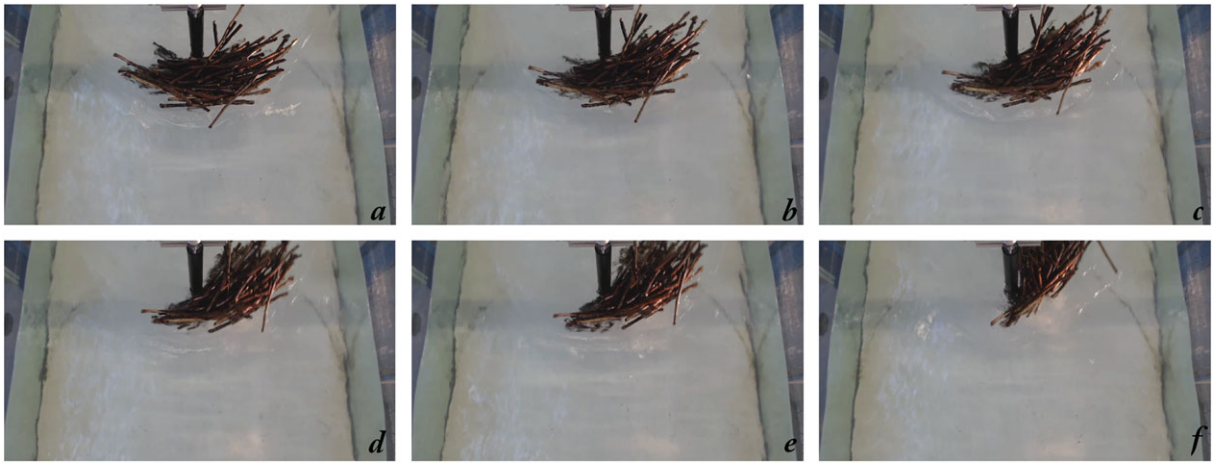

Figure 4. An example of accumulation failure for uniform size debris at the upstream face of the pier. The jam gradually rotates about the pier axis until it is completely dislodged from the pier and drifts away. (a) to (f) are taken with intervals of 1 s between each other.

the LWD pile has created a stable net of entangled elements, its width is subject to smaller and more gradual variations. The accumulation height follows the same tendency, although it reaches a more regular state later during the experiment. We classified this phase as a stable jam condition. During the development of this phase, the shape of all debris accumulations resembled a half-cone pointing downward, which results in a triangular cross section, although minor deviations were observed because of the inherent imperfection of geometric shapes formed by debris. The base of the jam is not circular as the values of K can differ significantly from $W/2$. Figure 3 shows a typical accumulation shape in this stable condition as observed by the three cameras. The cross section of the accumulation was found to be asymmetrical in all experiments when reaching the stable phase. Asymmetry is defined here as the condition in which the ratio between the left and right semiwidths W_L and W_R of the accumulation at the water surface (where W_L and W_R are, respectively, cross-sectional distances from the pier center to the left and right edges of the debris jam) is different than unity. Although the duration of each phase varied for each test, we clearly observed in all experiments that the

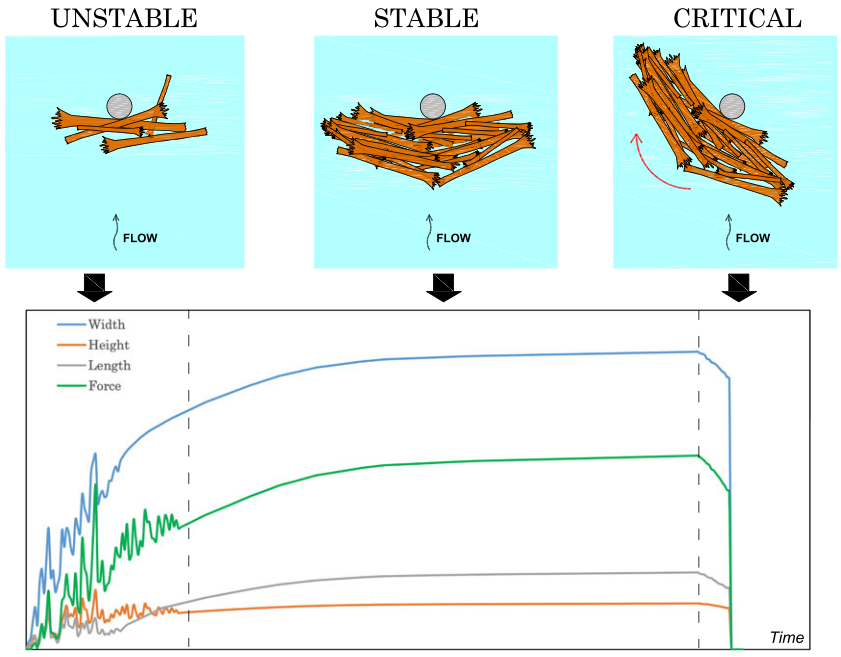

Figure 5. Sketch of the three growth phases typically observed in a jam. (top) Exemplified planar view. (bottom) Conceptualized plot based on actual data for growth in time of the main geometrical variables and of the applied force.

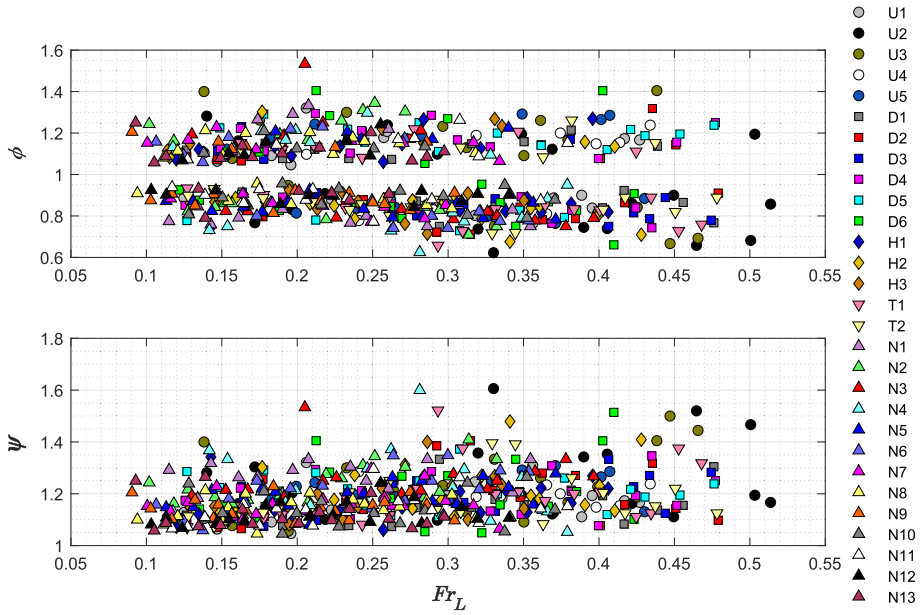

Figure 6. Asymmetry factors ϕ and ψ for all experiments against Fr_L. (top) $\phi = W_L/W_R$. (bottom) $\psi = W^c_{\max}/W^c_{\min}$.

stable condition lasted longer than the other two phases. Finally, the last stage (critical) is reached when the jam begins an oscillatory rotational movement about the pier. This motion occurs autonomously and was not observed to be driven by the impact of individual debris pieces (i.e., oscillations continue even if the supply of debris is stopped). During this phase, debris feeding continued uninterrupted. Eventually, these oscillations lead to the disengagement of the accumulation from the pier, which then drifts away. The dislodgement of the jam from the pier is hereafter indistinctively referred to as the failure or critical condition. The total number of elements forming the jam was counted after failure and ranged from 27 to 201. Figure 4 shows the final rotational sequence of an accumulation during the failure stage. The duration of this last phase varied for each test. At high flow conditions, failure occurred abruptly through a single and sudden rotation. Figure 5 shows a conceptualized example of the jam size growth in time and a sketch of the different stages observed during the lifetime of an accumulation, which together qualitatively represent the vast majority of accumulations observed.

The failure behavior described above was observed in all tests and began when W, H, and K were very close to their maximum values over the course of the experiment. Thus, the accumulation size at the onset of the critical stage can be regarded as a proxy for the maximum potential dimensions that modeled jams can reach, even though in some cases, they were not strictly maxima. This assumption is adopted in this paper, and values of width, height, and length measured at this critical stage (hereafter denoted by the superscript c) are assumed the maximum values obtained during the experiments. In all experiments, failure occurred as a rotation toward the side of the largest semiwidth. For instance, a jam as sketched in Figure 1 fails rotating clockwise if the semiwidth on the left side is greater than the semiwidth on the right side of the pier (i.e., $W_L > W_R$), otherwise it will rotate counterclockwise. The deepest point of the jam was observed at the pier face in almost all experiments. In order to understand the influence of asymmetry on failure, the asymmetry factors $\phi = W^c_L/W^c_R$ and $\psi = W^c_{\max}/W^c_{\min}$ (where $W^c_{\max}$ and $W^c_{\min}$ are, respectively, the largest and smallest of W^c_L and W^c_R) are introduced. The values of ϕ and ψ for all experiments with both uniform and nonuniform debris are plotted as a function of Fr_L in Figure 6. These results show that an accumulation generally fails at values of ϕ within the narrow range of approximately 0.7–0.95 and 1.05–1.3 (ψ between 1.05 and 1.3) and that ϕ and ψ are also independent of Fr_L. No failure occurred for values of ϕ and ψ close to unity, which suggests that failure is caused by the moment of the drag force induced by asymmetry. In addition, no noticeable differences are observed between uniform and nonuniform debris. Finally, it has been observed that flow

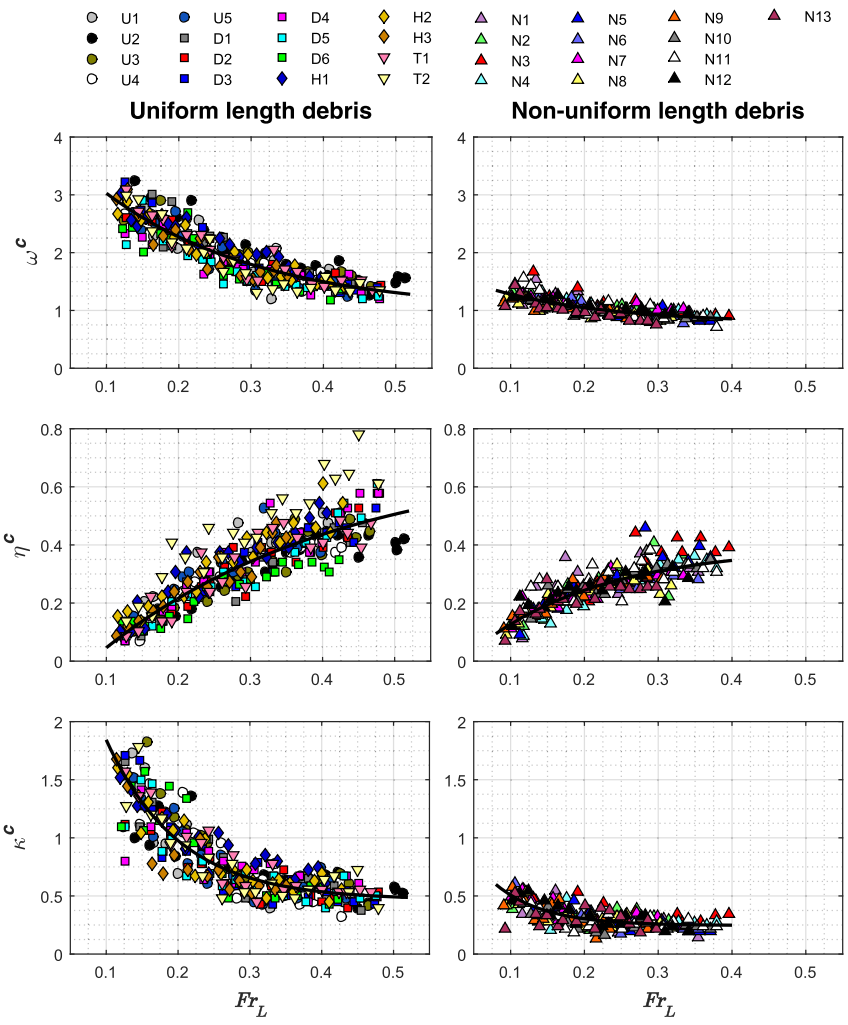

Figure 7. Critical values of the dimensionless (top to bottom) width ω^c, height η^c, and length κ^c against Fr_L (horizontal axis) for uniform (left) and nonuniform (right) debris tests. The black lines represent regression curves proposed for each data set.

conditions distinctly affect the lifetime of a woody debris jam, substantially reducing the time of all phases with increasing Fr_L.

The following sections will separately analyze the relations between the potential geometry of debris jams (represented by ω^c, η^c, and κ^c) and flow and debris characteristics for uniform and nonuniform debris.

4.1. Uniform Size Debris

Figure 7 (left) shows the three relations between the variables characterizing the critical geometry of the debris accumulations (ω^c, η^c, and κ^c) and Fr_L for all experiments with uniform debris, that is, groups U1 to U5, D1 to D6, H1 to H3, and T1 to T2. The figure also includes the regression curves that are discussed in section 5. The figure shows a clear dependency of the geometry of accumulations on flow, with all values clustered within a relatively narrow band. At low Fr_L, the critical width is the largest, reaching a value of 2.5 to 3 times the length of an individual debris element (i.e., $\omega^c = 2.5$ to 3). The value of ω^c gradually decreases with Fr_L up to $\omega^c \approx 1.5$ for the highest values of Fr_L tested. An opposite trend is observed for the dimensionless height η^c, which displays a sharp increase with increasing Fr_L. Namely, η^c values vary from around 0.1 at $Fr_L < 0.15$ up to $\eta^c \approx 0.5$ at $Fr_L \approx 0.47$. In other words, the cross-sectional shape of the accumulations changes from wide and superficial for low Fr_L values to narrow and deep with increasing Fr_L. The dimensionless streamwise length of the accumulation κ^c gradually drops with increasing Fr_L down to an average value of approximately $\kappa^c = 0.5$.

Unlike flow velocity and debris length, the effects of other variables on LWD accumulations are generally limited. Results in Figure 7 reveal that the influence of the dimensionless variable λ on the accumulation growth

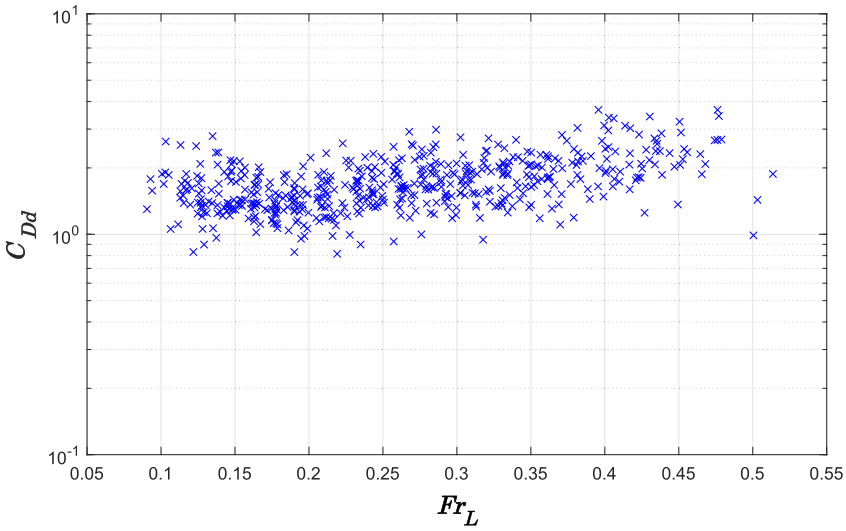

Figure 8. Drag coefficient C_{Dd} values as a function of Fr_L for all experiments.

is minimal for uniform debris. Although λ was varied between 3.75 (group U1) and 15 (group U5), values of ω^c, η^c, and κ^c are all clustered within a narrow band. In other words, for a given size of debris, the influence of the pier diameter D on the accumulation size is negligible within the range of values of λ tested in this study. Likewise, experimental groups D1 to D6 (for a total of 126 experiments) analyzed the effects of varying d/L on the dimensions of the formed debris jam. As can be observed in Figure 7, data are well-clustered around the same range of values for any d/L tested, and no trend can be noticed. The influence of the relative water depth h/L was studied by groups H1–H3. Figure 7 shows that no significant trend in the dimensions of the jams can be observed to occur as a function of h/L. Finally, results of the experiments with different debris densities have shown no noticeable relations between the horizontal dimensions ω^c and κ^c and the relative density ρ_L/ρ. Nonetheless, as shown in Figure 7, T2 tests displayed values of η^c up to 30% greater than those with smaller ρ_L/ρ, while T1 experiments followed the general trend.

4.2. Nonuniform Size Debris

Results for the critical width ω^c, height η^c, and length κ^c for all 13 groups of experiments performed with nonuniform length debris (N1 to N13 on Table 1) are also presented on Figure 7 (right), along with the corresponding regression curves. Similarly to the results of the uniform debris tests, ω^c and κ^c decrease, whereas η^c increases with increasing Fr_L. The highest values of ω^c range approximately between 1.1 and 1.5 at low Fr_L and decrease down to around 0.8–1 for the highest values of Fr_L tested. For $Fr_L > 0.25$, an important number of experiments displayed values of ω^c below 1, that is, the accumulation width is smaller than the length of the key element. This occurs because the key element is tilted from its initial position perpendicular to the flow, resulting in a smaller cross-sectional width. The dimensionless height η^c shows small values (around 0.1) for low Fr_L and then increases with Fr_L up to $\eta^c \approx 0.4$. As previously observed for the uniform debris, the dimensionless length κ^c decreases with increasing Fr_L, ranging from approximately 0.4–0.6 at the lowest to 0.2–0.3 at the highest values of Fr_L tested.

Interesting insights into the influence of the distribution of debris length on the critical geometry of accumulations can be obtained by comparing the values of ω^c, η^c, and κ^c in uniform and nonuniform experiments from Figure 7. This comparison shows that under the same Fr_L, the potential width of a debris jam formed with nonuniformly distributed debris is considerably smaller than the corresponding width of a uniform debris jam. In particular, at low values of Fr_L (around 0.1), observed values of ω^c were up to 2.5 times higher in the uniform than in the nonuniform experiments ($\omega^c \approx 3$ and $\omega^c \approx 1.2$, respectively). With increasing Fr_L, this difference is reduced (uniform $\omega^c \approx 1.5$ and nonuniform $\omega^c \approx 0.9$), although it is still high (i.e., the nonuniform debris accumulation is 40% smaller in width). The dimensionless height η^c reveals a less pronounced difference between nonuniform and uniform debris than ω^c. In particular, for low Fr_L, the nonuniform η^c tends to be slightly larger than in the uniform case. For higher Fr_L, this difference is inverted, and η^c for uniform debris is slightly larger than the nonuniform case. In the lower range of Fr_L, the values of κ^c observed in the nonuni-

form debris experiments were approximately one third of the corresponding κ^c values obtained with uniform debris, while at high Fr_L, the ratio between nonuniform and uniform κ^c values was approximately half.

4.3. Repeated Experiments

In order to understand the dispersion associated with the dynamics of debris accumulation and the predictability of the geometrical variables ω^c, η^c, and κ^c, one particular test was repeated 22 times using the same flow conditions and debris characteristics (debris from group N8, $L = 687.5$ mm, $D = 50$ mm, $Fr_L = 0.173$, and $\lambda = 13.75$). The mean value, standard deviation, and coefficient of variation (CV) of ω^c in these experiments were 1.0552, 0.1047, and 0.0992, respectively. The values of the same statistical parameters of η^c were 0.2036, 0.0491, and 0.2410, while κ^c displayed values of 0.3193, 0.0889, and 0.2784. The values of CV for ω^c denote a relatively small dispersion (less than 10%), whereas for η^c and κ^c, this is higher, indicating a greater degree of randomness for these two variables.

4.4. Forces Exerted on Woody Debris Jams

The force measured by the load cell allowed us to analyse of the drag force exerted on the woody debris accumulation. As expected, over the course of the experiments, drag evolves in time following a trend similar to the growth of the LWD jam. Namely, drag increases at a fast rate during the unstable phase of the jam growth, when it is subject to rapid changes that are clearly linked to the changes in the jam size. When the jam achieves the stable phase, the rate of change becomes milder and only dependent on the small changes of the jam size. During the critical phase, the oscillations of the woody debris pile induce a slight reduction and small variations in the measured force, until it eventually drops abruptly during the jam failure. During each individual test, the maximum drag force values were reached at the onset of the critical phase and are hereafter used for the estimation of the drag coefficient. A sketch of the temporal evolution of the drag force, together with jam size variables, is shown in Figure 5.

Figure 8 displays values of C_{Dd} for all experiments as a function of Fr_L. While dispersion is relatively high, at low Fr_L, most C_{Dd} values are within the range 1.0–2.0. No systematic differences have been observed in terms of the values of C_{Dd} for the different groups of experiments with uniform and nonuniform debris.

5. Discussion

The results of our experiments provide new insights into the evolution of debris accumulations at bridge piers. First, they show that the accretion is halted when a critical size is reached, after which a failure mechanism was observed in all tests. In addition, during all tests, the dimensions of the accumulations at this critical condition were either the highest or close to the highest. This provides an opportunity to define variables that for practical purposes represent the maximum dimensions that these accumulations can reach under given conditions of flow and a continuous supply of debris of given length. Previous studies on woody debris accumulations at bridges have not investigated the entire jam lifetime and therefore have not reported this key behavior. However, a field study by Lyn et al. (2007) noted that a few accumulations disappeared at some point, and in one case, they have proposed that the debris jam could have been disengaged from the pier and then transported and accumulated again downstream at another bridge pier. Our results provide strong evidence supporting this observation. The shape observed during our experiments was consistent with field observations by Diehl (1997), Abbe and Montgomery (2003), and Lagasse et al. (2010). Namely, the shape of the jams formed in all of our experiments resembled a half cone, with only minor deviations observed.

The results of our experiments have shown that failure always occurred when accumulations were asymmetric and through a rotation toward the widest side. This suggests that failure is caused by a shift in the center of application of the drag force from the pier axis toward the widest side. The observed values of the asymmetry factor ψ indicates that only a relatively small asymmetry is needed to drive failure (on average, failure was observed when the largest semiwidth was approximately 17% greater than the smallest). Values of ψ below 1.1 are rare, confirming that when the accumulation is almost or perfectly symmetrical (i.e., $\psi \approx 1$), failure is unlikely. On the other hand, lack of ψ values over 1.5 indicates that at these values cannot be formed because the failure rotation takes place before they can be reached.

The comparison of the size of accumulations that are formed by uniform and nonuniform debris has unveiled important differences. Although both show the same qualitative behavior, experiments with debris of uniform length produce accumulations that are considerably larger than those formed with a log-normal distribution of lengths having the same maximum length. This indicates that idealized laboratory tests with uniform size debris do not correctly represent real-world processes that take place in natural environments, where debris

is typically nonuniform. One exception to this rule may occur when the main supply of debris to the river comes from human activities that can produce more uniformly distributed sizes, such as logging. In spite of these considerations, uniform debris offer less complex experimental conditions that can be advantageous in the development of a mechanistic explanatory theory for the processes observed in this paper. It is also interesting to observe that the value of $\omega = 1$ proposed by Diehl (1997) based on field observations falls within our experimental results conducted with nonuniform debris ($\omega^c = 1$ for $Fr_L \approx 0.25$). However, our results show that ω^c can reach values approximately between 0.8 and 1.4 depending on Fr_L.

The results of the experiments with both uniform and nonuniform debris reveal clear relations between the three variables characterizing the geometry of accumulations ω^c, η^c, κ^c, and Fr_L. Furthermore, results clearly indicate that the length of individual debris elements L is key for determining the potential size reached by LWD piles, as previously suggested by field observations (Diehl, 1997). Results also showed that for practical purposes, the jam maximum size can be assumed independent of λ, d/L, and h/L within the range of values tested in these experiments. For instance, the dimensionless group d/L displayed only modest effects on the dimensions of the accumulations. The dimensionless water depth h/L showed no influence on the geometry of the LWD accumulations, confirming observations by Lyn et al. (2003) that for h sufficiently high, its effects on the debris jam growth are null. Lyn et al. (2003) observed that this variable can have an influence on the accumulation process at shallow depths, in which case, the accumulation would get anchored at the river bed. In this study, all tests were performed with enough water depth to prevent any interaction between debris and flume bed. Likewise, pier diameter D and debris length L were varied resulting in a wide range of the λ variable, but no noticeable influence on the geometry of the formed accumulations was observed. As a result, for the range of conditions analysed in this study, the influence of d/L, h/L, and D/L is minimal and can be neglected from the functional relation (3). Similar considerations are partially applicable to the dimensionless debris density ρ_L/ρ. While ρ_L/ρ has no effects on ω^c and κ^c, its influence on η^c is important as for the highest debris density, the accumulation depth was significantly higher than other tests with smaller ρ_L/ρ values. In the following analysis, this influence of ρ_L/ρ on η^c is neglected, and as a consequence, these results are strictly valid only for values of ρ_L within our experimental range of 450–550 kg/m^3. Experimental results have also clarified the influence of the ratio B/L on the accumulation process. Despite varying L between 0.250 and 0.375 m (for uniform debris) and between 0.375 and 0.750 m (for nonuniform debris), the debris jam formation mechanism and maximum size achieved were not systematically affected by changes of B/L. Thus, the dimensionless group B/L can be relaxed from (3) under our experimental conditions. Furthermore, results showed that there was negligible influence from the interaction with the walls on the accumulation process. The width blockage ratio was $0.26 < W^c/B < 0.70$ in most (90%) experiments. Higher values of W^c/B were formed only in a few tests (i.e., $0.70 < W^c/B \leq 0.87$ in only 10% of the experiments), but even within this higher range, no substantial differences in the dimensionless variables ω^c, η^c, and κ^c have been observed for different W^c/B values. For example, at low Fr_L in Figure 7, results for groups U1, U2, U3, and D3 display similar values of W^c/L despite substantially different values of W^c/B across these points. The amount of data at high values of W^c/B is however limited, and further tests are needed to determine the influence of this variable on the dimensions of debris accumulations (i.e., for nonisolated piers).

Under the above assumptions and further assuming that ω^c, η^c, and κ^c are mutually independent, the functional relation (3) can be simplified as

$$\mathbf{G} = \mathbf{F}(Fr_L), \tag{8}$$

where $\mathbf{G} = [\omega^c, \eta^c, \kappa^c]^T$ is the vector representing the critical geometry of the accumulation, and $\mathbf{F} = [f_1(Fr_L), f_2(Fr_L), f_3(Fr_L)]^T$ is the vector function, the components of which are functions defined by the three curves shown on Figure 7 for uniform (regression of all results except tests T1 and T2) and nonuniform debris, respectively. Equation (8) enables predictions of the potential dimensions of debris accumulations to be made as a function of the length of debris supplied from upstream and the approach flow velocity. This assumes that the accumulation is *supply unlimited* (i.e., the river or stream provides enough floating debris for the processes observed in this paper to develop) and that the hydrological event is long enough for a jam critical stage to be reached. This therefore represents a worst-case scenario that can be useful to assess horizontal loadings and afflux under extreme conditions. The results of the regression analysis of the data presented on

Figure 7 (uniform debris) yields the following three components of **F**:

$$\begin{aligned} \omega^c &= 0.988 + 3.238e^{-4.625Fr_L}, \\ \eta^c &= 0.703 - 0.887e^{-3.004Fr_L}, \\ \kappa^c &= 0.466 + 3.720e^{-9.936Fr_L} \quad \text{for } 0.11 < Fr_L < 0.51. \end{aligned} \tag{9}$$

The corresponding regression of the nonuniform length debris results in

$$\begin{aligned} \omega^c &= 0.774 + 0.939e^{-6.139Fr_L}, \\ \eta^c &= 0.394 - 0.458e^{-5.770Fr_L}, \\ \kappa^c &= 0.246 + 1.178e^{-15.039Fr_L} \quad \text{for } 0.10 < Fr_L < 0.40. \end{aligned} \tag{10}$$

An analysis of these regressions has been performed in order to assess whether correlation is strong and results are significant. To this end, the relations presented in Figure 7 have first been made linear by mapping $Fr_L \rightarrow e^{-cFr_L}$, where c is the parameter used for each of the regressions in (9) and (10). The values of the coefficient of determination R^2 for equations (9) in the mapped space were 0.82, 0.79, and 0.77 for ω^c, η^c, and κ^c respectively, which suggest a very strong correlation. The corresponding values of R^2 found for the nonuniform tests from equation (10) were 0.60, 0.69, and 0.45, which indicate a moderately strong correlation for ω^c and η^c and a moderate correlation for κ^c. A p value test carried out for each variable yielded p values well below the significance level of $\alpha = 0.01$ in any case, which suggests that our results are statistically significant. In addition, analysis of results from group R1 provided an assessment of dispersion of ω^c, η^c, and κ^c. While this analysis has been undertaken only for one particular set of experimental conditions, the inspection of results on Figure 7 provides no evidence of substantial changes in dispersion for particular experimental conditions.

These regressions can be regarded as a first attempt for estimating potential dimensions of LWD accumulations at bridge piers. While equations (9) and (10) both display similar trends, uniform length debris achieve jams that are substantially larger than those formed by nonuniform elements. In most real-world situations, (10) should be used to model a woody debris accumulation. However, (9) could be adopted to simulate certain scenarios involving the supply of debris of approximately uniform length (e.g., in areas subject to logging or harvesting). It is important to highlight that the relations above have been derived from experiments conducted in a straight prismatic flume in which the pier was located at the center of the rectangular cross section. Therefore, strictly speaking equations (9) and (10) are only valid under similar conditions. Flow in rivers can display complex patterns such as secondary currents that are likely to influence the processes of formation, growth and failure of debris jams at piers. It is unclear how these effects will influence the critical dimensions of accumulations formed under these conditions.

The analysis of the drag coefficient presented in Figure 8 completes the set of variables necessary to determine the drag force exerted on a debris jam. In our work, the large majority of C_{Dd} values is gathered between 1 and 2. These results are consistent with a preliminary experimental work by Parola et al. (2000), who examined the forces that can be exerted by LWD on a pier in laboratory tests using different jam models (flat plates, solid cones, and model debris elements). The present study provides further evidence and a substantially larger data set than Parola et al. (2000). Nevertheless, the values of the drag coefficient reported here should be used with caution. Parola et al. (2000) observed that C_{Dd} decreases with an increase in the blockage ratio (i.e., the ratio between the obstructed area and the free flow area) when this ratio exceeds 36%. In our experiments the values of the blockage ratio were much smaller (the maximum value was smaller than 20%), therefore representing the condition of an isolated pier. In addition, the dispersion observed in Figure 8 highlights the difficulties in obtaining accurate and consistent predictions of C_{Dd} from laboratory experiments of debris accumulations.

6. Conclusions

Understanding the phenomenon of woody debris jams at bridge piers is of primary importance for assessing of the risk of bridge collapse and flooding, as well as for the design of new bridges. This article provides a detailed experimental analysis of the whole life of debris accumulations at bridge piers including their formation, growth, and failure. Our observations unveiled three distinct stages that are conceptually classified as unstable, stable, and critical conditions. The unstable phase occurs at the beginning of the recruitment process, when a debris framework is formed and the accumulation displays a rapid growth. During this phase,

individual debris elements are easily disengaged and drift downstream. Once a robust framework is formed, a stable phase is observed during which only moderate changes in the accumulation structure occur and the jam either does not grow or grows at a slow pace. Finally, the critical phase denotes the final stage of a debris accumulation when an oscillatory rotational movement is observed, which eventually leads to the failure of the accumulation (i.e., complete removal from the pier). The observation that all debris accumulations fail is particularly important, as this failure condition can be used to define metrics to characterize the dimensions of potentially large accumulations. In fact, in almost all experiments, these oscillations began when the size of the debris jam was maximum. The three dimensions thus defined (i.e., width W^c, height H^c, and length K^c, and the respective variables made dimensionless with the length of debris element ω^c, η^c, and κ^c) have been analyzed for different flow conditions and debris sizes, including experiments with uniform and nonuniform distributions of debris length.

Results have shown a clear dependency of the accumulation dimensions on the dimensionless parameter $Fr_L = v/(gL)^{0.5}$. For low values of Fr_L, ω^c and κ^c are the highest, while dimensionless height η^c is the smallest. ω^c and κ^c were observed to decrease with increasing Fr_L, while η^c displays the opposite trend. Under the experimental conditions studied in this article, the diameter of the circular piers was observed to have negligible influence on the values of ω^c, η^c, and κ^c. Namely, values of ω^c, η^c, and κ^c obtained in all experiments were clustered within a narrow band for values of $\lambda = L/D$ ranging from 3.5 to 30. In a similar way, the dimensionless debris diameter d/L and water depth h/L displayed no notable effects on the maximum size achieved by an accumulation within the studied range. The relative debris density ρ_L/ρ had no influence on the width ω^c and length κ^c of the accumulations. However, the experiment performed with the highest value of ρ_L/ρ resulted in a accumulation that was up to 30% deeper than those formed with the lowest values of ρ_L/ρ.

A comparison between the dimensions of debris jams formed with uniform and nonuniform distributions of the length of individual debris elements has shown considerable differences. Accumulations formed by single-sized debris are notably larger than those formed by log-normally distributed debris of equal maximum length. This indicates that idealized experiments with uniform debris length will overestimate accumulations that are likely to be formed in the real-world, where debris is typically nonuniform in size.

The relations provided in this paper enable the estimation of the potential size and shape that debris accumulations can reach for given flow conditions and characteristics of floating debris transported by the stream. In addition, an estimation of the drag coefficient of debris jams was provided. These relations pave the way for a number of practical applications that in the past have been hindered by a lack of understanding of the dynamics of debris accumulations and the absence of predictive methods. These include the effects of debris jams on upstream water levels during floods as well as the estimation of horizontal loadings exerted by debris on piers, which is of primary importance for assessing the risk of failure of existing bridges and for the design of new ones.

Acknowledgments
The authors are grateful for the financial support of the Engineering and Physical Sciences Research Council (EPSRC) through the Centre for Doctoral Training in Sustainable Infrastructure Systems (CDT-SIS), grant EP/L01582X/1. Part of this research was also funded under UK Natural Environment Research Council grant NE/R009015/1. Finally, we would like to thank Dr Toru Tsuzaki and Mr Karl Scammell of the University of Southampton Hydraulics Laboratory for the technical and material support in carrying out the experiments. Data supporting the results presented in this paper are openly available from the University of Southampton repository at doi: http://doi.org/10.5258/SOTON/D0057.

References

Abbe, T. B., & Montgomery, D. R. (1996). Large woody debris jams, channel hydraulics and habitat formation in large rivers. *Regulated Rivers Research & Management*, *12*, 201–221.

Abbe, T. B., & Montgomery, D. (2003). Patterns and processes of wood debris accumulation in the Queets river basin, Washington. *Geomorphology*, *51*, 81–107.

Benn, J. (2013). Railway bridge failure during flooding in the UK and Ireland. *Proceedings of the Institution of Civil Engineers*, *166*(4), 163–170.

Blersch, D. M., & Kangas, P. C. (2014). Signature of self-assembly in size distributions of wood members in dam structures of Castor canadiensis. *Global Ecology and Conservation*, *2*, 204–213.

Bocchiola, D., Rulli, M., & Rosso, R. (2008). A flume experiment on the formation of wood jams in rivers. *Water Resources Research*, *44*, W02408. https://doi.org/10.1029/2006WR005846

Bradley, J. B., Richards, D. L., & Bahner, C. D. (2005). *Debris Control Structures—Evaluation and Countermeasures*. Washington D. C., USA: U.S Department of Transportation, Federal Highway Administration.

Braudrick, C. A., Grant, G. E., Ishikawa, Y., & Ikeda, H. (1997). Dynamics of wood transport in streams: A flume experiment. *Earth Surface Processes and Landforms*, *22*, 669–683.

Diehl, T. H. (1997). *Potential Drift Accumulation at Bridges*. Washington D.C., USA: Federal Highway Administration, U.S. Department of Transportation.

Gippel, C., O'Neill, I., Finlayson, B., & Schnatz, I. (1996). Hydraulics guidelines for the reintroduction and management of large woody debris in lowland rivers. *Regulated Rivers Research & Management*, *12*, 223–236.

Gschnitzer, T., Gems, B., Mazzorana, B., & Aufleger, M. (2017). Towards a robust assessment of bridge clogging processes in flood risk management. *Geomorphology*, *279*, 128–140.

Hess, J. (2007). Distribution and residence times of large woody debris along South River (Master's Thesis), University of Delaware, Shenandoah Valley, Virginia.

Hygelund, B., & Manga, M. (2003). Field measurements of drag coefficients for model large woody debris. *Geomorphology*, *51*, 175–185.

Lagasse, P., Colopper, P., Zevenbergen, L., Spitz, W., & Girard, L. (2010). *Effects of Bebris on Bridge Pier Scour*. Washington D.C., USA: National Cooperative Highway Research Program Transportation Research Board.

Lyn, D., Cooper, T., Condon, C., & Gan, G. (2007). *Factors in Debris Accumulation at Bridge Piers*. Washington D.C., USA: Federal Highway Administration, U.S. Department of Transportation.

Lyn, D., Cooper, T., Yi, Y., Sinha, R., & Rao, A. (2003). *Debris accumulation at Bridge Crossing: Laboratory and Field Studies*. Washington D.C., USA: Federal Highway Administration, U.S Department of Transportation.

Manners, R. B., & Doyle, M. W. (2008). A mechanistic model of woody debris jam evolution and its application to wood-based restoration and management. *River Research and Applications*, *24*, 1104–1123.

Manners, R. B., Doyle, M. W., & Small, M. J. (2007). Structure and hydraulics of natural woody debris jams. *Water Resources Research*, *43*, W06432. https://doi.org/10.1029/2006WR004910

Melville, B. W., & Dongol, D. (1992). Bridge pier scour with debris accumulation. *Journal of Hydraulic Engineering*, *118*, 1306–1310.

Pagliara, S., & Carnacina, I. (2011). Influence of wood debris accumulation on bridge pier scour. *Journal of Hydraulic Engineering*, *137*, 254–261.

Pagliara, S., & Carnacina, I. (2013). Bridge pier flow field in the presence of debris accumulation. *Proceedings of the Institution of Civil Engineers*, *166*(4), 187–198.

Panici, D., & de Almeida, G. A. M. (2017). Understanding woody debris jams at bridge piers. In *Proceedings of the 37th IAHR World Congress: Managing Water for Sustainable Development, learning from the Past for the Future*, Kuala Lumpur, Malaysia, pp. 1404–1411.

Parola, A. C., Apelt, C. J., & Jempson, M. A. (2000). *Debris Forces on Highway Bridges*. Washington D. C., USA: National Cooperative Highway Research Program Transportation Research Board.

Pfister, M., Capobianco, D., Tullis, B., & Schleiss, A. J. (2013). Debris-blocking sensitivity of piano key weirs under reservoir-type approach flow. *Journal of Hydraulic Engineering*, *139*, 1134–1141.

Ruiz-Villanueva, V., Badoux, A., Boes, R. M., Rickenmann, D., Rickli, C., Schalko, I., et al. (2016). Large wood research in Swiss watercourses. In G. Constantinescu, et al. (Eds.), *Proceedings of the International Conference on Fluvial Hydraulics* (pp. 2307–2314). Boca Raton: CRC Press.

Rusyda, M., Hashimoto, H., & Ikematsu, S. (2014). Log jam formation by an obstruction in a river, *Proceedings of the International Conference on Fluvial Hydraulics, RIVER FLOW 2014*. Lausanne, Switzerland: CRC Press/Balkema, pp. 717–724.

Schmocker, L., & Hager, W. H. (2011). Probability of drift blockage at bridge decks. *Journal of Hydraulic Engineering*, *137*, 470–479.

Sedell, J., Bisson, P., & Gregory, S. (1988). From the forest to the sea: A story of fallen trees, *Chapter 3. What We Know About Large Trees that Fall into Streams and Rivers*: U.S. Department of Agriculture, Forest Service, Pacific Northwest Research Station; U.S. Department of the Interior, Bureau of Land Management Portland.

Tritton, D. J. (1977). *Physical Fluid Dynamics*. Berkshire, England: Van Nostrand Reinhold Wokingham.